Estimation of total attenuation and scatterer size from backscattered ultrasound waveforms

Timothy A. Bigelow, Michael L. Oelze, and William D. O'Brien, Jr.[a)]
Bioacoustics Research Laboratory, Department of Electrical and Computer Engineering, University of Illinois, 405 North Mathews, Urbana, Illinois 61801

(Received 7 September 2004; revised 15 December 2004; accepted 22 December 2004)

Quantitative ultrasound techniques using backscattered echoes have had limited success *in vivo* due to the frequency-dependent attenuation along the entire propagation path masking the frequency dependence of the backscatter. Herein, total attenuation and scatterer size are estimated simultaneously by an analysis of the *in vivo* backscattered power spectrum using two approaches. The simulations used to evaluate the two approaches used frequencies between 4 and 11 MHz with an effective scatterer radius of 25 μm. The first approach was based on approximations of the *in vivo* backscattered power spectrum (i.e., assumed Gaussian function), wherein attenuation and size were estimated by assuming each was a Gaussian transformation performed on Gaussian power spectra. The approach had poor accuracy due to the backscattered power spectra not being sufficiently modeled by a Gaussian function. The second approach estimated attenuation and size by fitting a modified reference spectrum to the *in vivo* backscattered power spectrum without any assumptions about the shape of the spectrum. The accuracy of the size estimate was better than 20% for signal-to-noise ratio >6 dB, window lengths greater than 4 mm, and attenuation between 0 and 1 dB/cm-MHz. However, the precision quickly degraded with increasing noise, increasing attenuation, and decreasing window length.
[DOI: 10.1121/1.1858192]

PACS numbers: 43.80.Ev, 43.80.Qf, 43.80.Vj [FD] Pages: 1431–1439

LIST OF SYMBOLS

A	term for form factor written as a power law [i.e., $F_\gamma(f,a_{\text{eff}})\cong e^{-Af^n}$]
a_{eff}	effective radius of scatterer
$a_{\text{eff}\,j}$	estimated effective radius of scatterer found from one set (i.e., 25 averaged rf echoes) of simulated backscatter waveforms
$\overline{a}_{\text{eff}}$	mean value of estimated effective radius from all sets of backscattered waveforms (i.e., $\overline{a}_{\text{eff}}=\Sigma_{\forall j}a_{\text{eff}\,j}/\Sigma_{\forall j}j$)
ASD	average squared difference term minimized by spectral fit algorithm
c	speed of sound in the tissue
c_o	speed of sound in water
$E[\ ]$	expected value with respect to scattering random process
$E_N[\ ]$	expected value with respect to electronic noise random process
f	frequency
$f\#$	f number of a focused transducer
f_o	the frequency corresponding to the spectral peak of the Gaussian spectrum [i.e., $\exp(-([(f-f_o)/\sqrt{2}\sigma_\omega])^2)$]
$\tilde{f}_o$	f_o for backscattered spectrum modified by scatterer size
$\tilde{f}'_o$	f_o for backscattered spectrum modified by scatterer size and attenuation along propagation path
$F_\gamma(\omega,a_{\text{eff}})$	form factor related to the scatterer geometry and size
g_{win}	windowing function used to gate the time-domain waveforms
$H(f)$	one-way passband characteristics of ultrasound source
k	wave number in tissue
k_o	wave number in water
L	length of the windowing function
n	power of frequency when form factor is written as a power law [i.e., $F_\gamma(f,a_{\text{eff}})\cong e^{-Af^n}$]
$N_{\text{space}}(f)$	spectral fluctuations from random scatterer spacing
$N(f)$	spectrum of additive electronic noise
P_{ref}	reference spectrum. [i.e., $P_{\text{ref}}(f)=k_o^4\lvert V_{\text{inc}}(\omega)\rvert^2\lvert H(\omega)\rvert^4$]
P_{scat}	$E[\lvert V_{\text{refl}}\rvert^2]$ estimated from set of waveforms ($\neq E[\lvert V_{\text{refl}}\rvert^2]$ due to the finite number of waveforms available to generate the estimate)
SNR	signal-to-noise ratio
t	time
T_{win}	length windowing function applied to time-domain waveform (i.e., $T_{\text{win}}=2L/c$)
V_{inc}	voltage spectrum applied to ultrasound source
V_j	backscattered voltage spectrum for a single rf echo
v_{noise}	noise signal voltage in time domain (i.e., no signal transmitted by source)
V_{plane}	backscattered voltage spectrum from rigid plane placed at the focal plane [i.e., proportional to $V_{\text{inc}}(\omega)(H(\omega))^2e^{i2k_oz_T}$]

[a)]Electronic mail: wdo@uiuc.edu

V_{refl} backscattered voltage spectrum from tissue containing scatterers

$v_{\text{refl}\,j}$ voltage of a rf echo in time domain

w_x, w_y, w_z equivalent Gaussian dimensions of velocity potential field in focal region

X, $\bar{X}$ terms used in minimization scheme for spectral fit algorithm

z_T distance from aperture plane to focal plane of ultrasound source

α total effective attenuation coefficient for tissue between ultrasound source and the region containing the scatterers (i.e., assumed linear frequency dependence of the form $\alpha = \alpha_o f + \alpha_b$)

α_b intercept of total attenuation coefficient at zero frequency

α_o slope of total attenuation coefficient versus frequency

$(\alpha_o z_T)_j$ estimated attenuation along the propagation path for single data set

$\overline{(\alpha_o z_T)}$ mean value for attenuation along the propagation path from all sets of backscattered waveforms [i.e., $\overline{(\alpha_o z_T)} = \Sigma_{\forall j}(\alpha_o z_T)_j / \Sigma_{\forall j} j$]

$\sigma_{a_{\text{lower}}}$ percent deviation in values of scatterer size for sizes smaller than the mean size (i.e., $a_{\text{eff}\,j} < \overline{a_{\text{eff}}}$)

$\sigma_{a_{\text{upper}}}$ percent deviation in values of scatterer size for sizes larger than the mean size (i.e., $a_{\text{eff}\,j} > \overline{a_{\text{eff}}}$)

$\sigma_{\alpha_{\text{lower}}}$ deviation in dB/MHz in values of attenuation for attenuation values smaller than the mean attenuation [i.e., $(\alpha_o z_T)_j < \overline{(\alpha_o z_T)}$]

$\sigma_{\alpha_{\text{upper}}}$ deviation in dB/MHz in values of attenuation for attenuation values greater than the mean attenuation [i.e., $(\alpha_o z_T)_j > \overline{(\alpha_o z_T)}$]

σ_ω the bandwidth term for Gaussian function [i.e., $\exp(-([(f-f_o)/\sqrt{2}\sigma_\omega])^2)$]

$\tilde{\sigma}_\omega$ σ_ω for backscattered spectrum modified by scatterer size

ω, λ radian frequency, wavelength

I. INTRODUCTION

For years many investigators have attempted to quantify the ultrasound backscatter from tissue by analyzing the power spectra of the rf echoes to estimate the characteristic size of the tissue microstructure (Lizzi *et al.*, 1983; Nassiri and Hill, 1986; Insana *et al.*, 1990; Hall *et al.*, 1996; Oelze *et al.*, 2004). The hypothesis is that the size of the tissue microstructure (i.e., scattering sources) could be used to assess the pathology of the imaged region. For example, researchers have verified that the backscattered power spectrum can be used to distinguish between fibroadenomas and carcinomas (Oelze *et al.*, 2004), as well as to monitor tissue necrosis in ultrasound therapy applications (Lizzi *et al.*, 1997). In light of these successes, it is suggested that the quantitative ultrasound (QUS) estimate of the characteristic size of the tissue microstructure could assist both diagnosis and treatment of pathological tissue.

Unfortunately, the scatterer size estimate has had limited success in clinical practice. The inability to apply laboratory measurements to a clinical setting is due primarily to a false assumption in the traditional estimation routine. Namely, it has been assumed that the total attenuation along the entire propagation path is the same for every patient and is known *a priori* (Oelze and O'Brien, 2002a). If known, the *in vivo* backscattered power spectrum can be compensated for the frequency-dependent attenuation, and the scatterer size can be accurately estimated assuming the scattering process is accurately modeled. However, the attenuation coefficient and thickness of different intervening tissue layers (i.e., fat, muscle, etc.) vary between patients. Lu *et al.* (1999) and Hall *et al.* (1996) attempted to improve the *in vivo* estimate by measuring the thickness of the different intervening tissue layers from the backscattered signals and assigning typical attenuation values to each layer. However, they did not account for the natural variability in attenuation for tissues of the same type. For example, Goss *et al.* (1978) report many different attenuation coefficients of fat taken at different frequencies. In particular, a study by Dussik and Fritch (1956) gives attenuation values of 0.6 ± 0.2 dB/cm at 1 MHz, 1.6 ± 0.2 dB/cm at 3 MHz, and 2.3 ± 0.7 dB/cm at 5 MHz. Hence, the slope of the attenuation versus frequency would vary from 0.2 to 0.65 dB/cm-MHz with a mean value of 0.43 dB/cm-MHz for that study alone. Lu *et al.* (1999) used a value of 0.6 dB/cm-MHz for the attenuation coefficient of fat while referring to Goss *et al.* (1978). However, it is not clear how this number was obtained from the data presented in Goss *et al.* (1978) because the attenuation slope was not measured directly over the diagnostic range in any of the studies presented. Clearly, there is significant variability in the attenuation slope. As a result, it is not feasible to determine accurately the characteristic size of the tissue microstructure of embedded tissues using the Lu *et al.* (1999) or Hall *et al.* (1996) technique.

The best successes clinically for scatterer size estimates were with tumors of the eye where the attenuation along the propagation path is negligible (Lizzi *et al.* 1983; 1997). Other investigators used scatterer size estimates to measure structural changes in the kidney (Insana *et al.*, 1995), where the exteriorized kidney reduced the impact of the attenuation along the propagation path.

Therefore, the frequency-dependent total attenuation along the propagation path must be determined on a patient-specific basis before the full potential of the estimation of scatterer size can be realized, as was recognized over 20 years ago by Lizzi *et al.* (1983). In addition to estimating the size of the tissue microstructure of embedded tumors and other pathologies, a knowledge of the attenuation along the propagation path could improve other medical ultrasound applications including acoustic radiation force impulse imaging (Nightingale *et al.*, 2000) and patient-specific dosimetry (Siddiqi *et al.*, 1992).

Due to the need and significant benefit of an accurate estimate of the total attenuation along the propagation path when quantifying tissue microstructure using ultrasound, as well as other applications, two different algorithms are explored herein. The two algorithms provide an estimate of total attenuation and scatterer size simultaneously from the

in vivo backscattered power spectrum. The algorithms represent two approaches. The first algorithm, termed the Gaussian transformation (GT) algorithm, was based on an approximation regarding the shape of the *in vivo* backscattered power spectrum and determined the scatterer size and total attenuation from two independent properties of the backscattered spectrum (i.e., center frequency and bandwidth). The second algorithm, termed the spectral fit (SF) algorithm, made no approximations about the shape of the *in vivo* backscattered power spectrum and solved for the size and attenuation by performing a fit over the entire frequency spectrum, similar to the established method for determining just the scatterer size when the attenuation is known (Insana *et al.*, 1990). Both algorithms are first described and then evaluated using computer simulations where the scatterers have Gaussian impedance distributions (i.e., Gaussian scatterers, a form factor). However, the SF algorithm, and possibly the GT algorithm, can be implemented for scatterers with any form factor (i.e., spherical shell, fluid-filled sphere, etc.) provided that the form factor is known *a priori* just like the established method for determining only the scatterer size when the attenuation is known (Insana *et al.*, 1990). In addition to the algorithms, a method to compensate for electronic system noise is developed. After presenting and evaluating each of the algorithms, some conclusions are drawn based on the results.

II. GAUSSIAN TRANSFORMATION ALGORITHM

The goal of the GT algorithm was to estimate the scatterer size and total attenuation from the *in vivo* backscattered power spectrum. The algorithm assumes that the backscattered signal has a Gaussian distributed spectrum where the scatterer size and total attenuation are independent Gaussian transformations. The analysis is similar to that presented by Wear (2002), who used Gaussian transformations to predict the *in vivo* backscattered power spectrum for given scatterers and attenuation.

A. Overview of algorithm

The expected backscattered voltage, $E[|V_{\text{refl}}|^2]$, from a tissue region where the window length is small compared to the depth of focus (i.e., local plane-wave approximation), and the attenuation in the focal region does not significantly alter the spectrum over the length of the window given by (Bigelow and O'Brien, 2004)

$$E[|V_{\text{refl}}|^2] \propto k_o^4 |V_{\text{plane}}(\omega)|^2 e^{-4\alpha z_T} F_\gamma(\omega, a_{\text{eff}}). \tag{1}$$

Equation (1) can be further simplified by assuming that the total attenuation along the propagation path has a linear dependence on frequency (i.e., $\alpha = \alpha_o f + \alpha_b$), a reasonable assumption over the bandwidth of most ultrasound sources (Jongen *et al.*, 1986). Then, the frequency-independent component of the attenuation, α_b, only influences the magnitude of the backscattered spectrum and hence can be absorbed by the proportionality, and the attenuation has a strictly linear dependence on frequency.

For Gaussian scatterers, as well as possibly for other form factors over a limited frequency range, $F_\gamma(\omega, a_{\text{eff}})$ can be reasonably approximated as e^{-Af^n}. Therefore, if the source spectrum and diffraction characteristics can be assumed Gaussian (i.e., $k_o^4 |V_{\text{plane}}(\omega)|^2 \propto \exp(-[(f - f_o)^2/2\sigma_\omega^2])$), then the backscattered voltage is given by

$$E[|V_{\text{refl}}|^2] \propto e^{[(f-f_o)^2/2\sigma_\omega^2]} e^{-Af^n} e^{-4z_T\alpha_o f}, \tag{2}$$

or a series of Gaussian transformations operating on a Gaussian function. Equation (2) can be simplifed by writing Af^n as a Taylor series about f_o, which is

$$Af^n = A\sum_{l=0}^{\infty} \frac{n! f_o^{n-l}}{(n-l)!\,l!} (f - f_o)^l. \tag{3}$$

Also, if $2 \leqslant n < 3$, then the terms in the Taylor series corresponding to $l \geqslant 3$ can be ignored due to the negative power on f_o. For Gaussian scatterers (i.e., $n = 2$), the $l \geqslant 3$ terms are already zero so there is no error introduced by making this assumption for these scatterers. After eliminating the $l \geqslant 3$ terms, Eq. (2) becomes

$$E[|V_{\text{refl}}|^2] \propto \exp\left(-\frac{(f - \tilde{f}_o')^2}{2\tilde{\sigma}_\omega^2} + \cdots \right), \tag{4}$$

where

$$\begin{aligned} \tilde{f}_o &= f_o - \tilde{\sigma}_\omega^2 A n f_o^{n-1}, \\ \tilde{\sigma}_\omega^2 &= \left[\frac{1}{\sigma_\omega^2} + An(n-1) f_o^{n-2} \right]^{-1}, \\ \tilde{f}_o' &= \tilde{f}_o - 4z_T \alpha_o \tilde{\sigma}_\omega^2. \end{aligned} \tag{5}$$

Based on Eq. (4), the bandwidth of the backscattered spectrum is only affected by the scatterer size. Hence, the scatterer size can be determined independently of the attenuation by measuring changes in the bandwidth of the backscattered signals. Once the scatterer size has been determined, the backscattered spectrum can be multiplied by e^{+Af^n} to remove the effect of scatterer size. Then, the total attenuation can be determined from the downshift in the center frequency of the returned spectrum. Hence, the scatterer size and total attenuation can theoretically be determined from two different properties of the backscattered spectrum.

B. Simulation results

The performance of the GT algorithm was evaluated by simulations that were designed to test the algorithm's sensitivity as a function of attenuation. In all of the simulations, the ultrasound source was a spherically focused $f/4$ transducer with a focal length of 5 cm placed adjacent to a homogeneous semi-infinite half-space containing scatterers. The velocity potential field near the focus was assumed to follow a three-dimensional Gaussian function, an approximation shown to be valid for focused sources (Bigelow and O'Brien, 2004), with the equivalent Gaussian dimensions given by

$$\begin{aligned} w_x &= w_y = 0.87\lambda f\#, \\ w_z &= 6.01\lambda (f\#)^2. \end{aligned} \tag{6}$$

The source was excited by an impulse [i.e., $V_{\text{inc}}(f) = 1$], and had one-way passband characteristics given by (Bigelow and O'Brien, 2004)

$$H(f)=\frac{|f|\exp\left(-\left(\frac{f-8\ \text{MHz}}{6\ \text{MHz}}\right)^2\right)}{\max_{\forall f}\left(|f|\exp\left(-\left(\frac{f-8\ \text{MHz}}{6\ \text{MHz}}\right)^2\right)\right)}, \tag{7}$$

comparable to that measured for a PZT transducer that also goes to zero at zero frequency. The voltage spectrum returned from a plane placed at the focal plane would be given by

$$V_{\text{plane}}(\omega)\propto V_{\text{inc}}(\omega)(H(\omega))^2 e^{i2k_o z_T}. \tag{8}$$

The simulated source spectra and diffraction characteristics [i.e., $k_o^4|V_{\text{plane}}(\omega)|^2$] were not perfectly Gaussian, but instead went to zero at zero frequency, just like a real source. This was done so that reasonable deviations from the ideal theory could be assessed.

The backscattered voltage for the simulations was generated by solving for the scattered field from a single scatterer with a Gaussian impedance distribution [i.e., Gaussian scatterer with $F_\gamma(f,a_{\text{eff}})=\exp(-0.827(ka_{\text{eff}})^2)$] at an arbitrary location in the focal region. A Gaussian scatterer was selected because the microstructure of real tissue is often modeled using this form factor (Chaturvedi and Insana, 1996). The backscatter for many scatterers in the half-space was then obtained by adding together the backscatter from many different randomly positioned scatterers. In the simulations, the scatterers were positioned according to a uniform probability distribution throughout the focal region at a density of 35/mm^3 ($\sim$4.8 scatterers per resolution cell) and each scatterer had an effective radius, a_{eff}, of 25 μm. The sound speed for the half-space was 1532 m/s, a measured sound speed for liver (characteristic of tissue) (Goss *et al.*, 1978, 1980). The attenuation was uniform throughout the half-space and was varied between 0 and 1 dB/cm-MHz in order to test the algorithm's sensitivity to attenuation. The reflection off of the rigid plane at the focus was also simulated using a sound speed of 1540 m/s for the water path. The code used a ''digitizing'' sampling rate of 53 MHz with no added electronic noise.

For each value of attenuation, the backscattered voltage from 1000 independent random scatterer distributions was generated. The waveforms were then separated into 40 independent sets with 25 waveforms per set and windowed in the time domain using a Hamming gating function centered at the focus, thus yielding 40 independent estimates of the effective scatterer radius and the total attenuation. The use of 25 rf echoes is arbitrary, and increasing the number of waveforms may improve the accuracy and precision of the resulting estimates. The width of the Hamming window was varied from 1 to 8 mm in steps of 0.25 mm (i.e., 0.057 to 0.45 by 0.014 when normalized with respect to depth of focus at the center frequency of 9.83 MHz) with corresponding time gates determined from $T_{\text{win}}=2L/c$. The same length Hamming window relative to the wavelength (i.e., $T_{\text{win}}=2L/c_o$) was also used to window the signal returned from the rigid plane placed at the focus when obtaining the reference spectrum. No correction was made for the resulting convolution that would distort the estimates at small window length. The

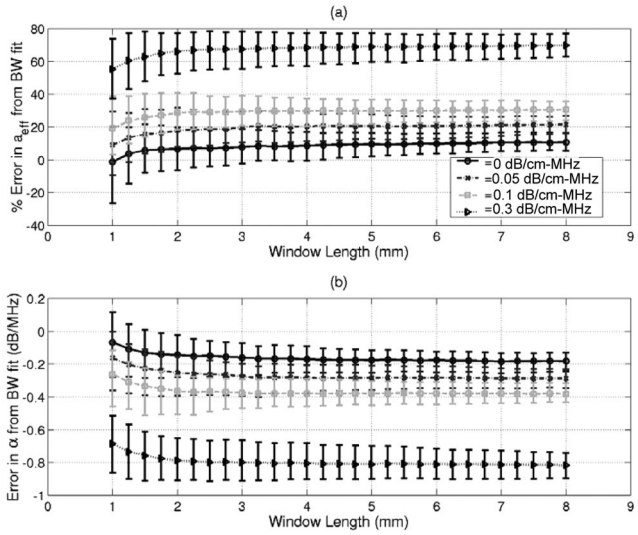

FIG. 1. (a) Percent error in scatterer radius and (b) error in total attenuation for semi-infinite half-spaces with attenuation values of 0, 0.05, 0.1, and 0.3 dB/cm-MHz using the Gaussian transformation algorithm.

resulting estimates from the GT algorithm for attenuation values of 0, 0.05, 0.1, and 0.3 dB/cm-MHz are shown in Fig. 1. The error bars in each case correspond to

$$\sigma_{a_{\text{apper}}}=\frac{100}{a_{\text{eff}|\text{Theory}}}\sqrt{\frac{\Sigma_{\forall a_{\text{eff}\,j}>\bar{a}_{\text{eff}}}(a_{\text{eff}\,j}-\bar{a}_{\text{eff}})^2}{\Sigma_{\forall a_{\text{eff}\,j}>\bar{a}_{\text{eff}}}j}},$$

$$\sigma_{a_{\text{lower}}}=\frac{100}{a_{\text{eff}|\text{Theory}}}\sqrt{\frac{\Sigma_{\forall a_{\text{eff}\,j}<\bar{a}_{\text{eff}}}(a_{\text{eff}\,j}-\bar{a}_{\text{eff}})^2}{\Sigma_{\forall a_{\text{eff}\,j}<\bar{a}_{\text{eff}}}j}}, \tag{9}$$

for the plots of error in a_{eff} and

$$\sigma_{\alpha_{\text{apper}}}=\sqrt{\frac{\Sigma_{\forall(\alpha_o z_T)_j>\overline{(\alpha_o z_T)}}((\alpha_o z_T)_j-\overline{(\alpha_o z_T)})^2}{\Sigma_{\forall(\alpha_o z_T)_j>\overline{(\alpha_o z_T)}}j}},$$

$$\sigma_{\alpha_{\text{lower}}}=\sqrt{\frac{\Sigma_{\forall(\alpha_o z_T)_j<\overline{(\alpha_o z_T)}}((\alpha_o z_T)_j-\overline{(\alpha_o z_T)})^2}{\Sigma_{\forall(\alpha_o z_T)_j<\overline{(\alpha_o z_T)}}j}}, \tag{10}$$

for the plots of error in total attenuation.

For small attenuation values, the scatterer size was estimated with reasonable accuracy (i.e., errors of $\sim$20%). However, as the attenuation was increased, the errors in the scatterer size estimate quickly grew and were $\sim$70% for an attenuation value of 0.3 dB/cm-MHz. The errors were even larger for the higher attenuation values (not shown in this plot). This increase in error with increasing attenuation resulted from a breakdown in the assumption that the source and diffraction characteristics [i.e., $k_o^4|V_{\text{plane}}(\omega)|^2$] followed a Gaussian function. For a Gaussian spectrum, the only change in the bandwidth of the Gaussian spectrum would be due to the size of the scatterer. However, the spectrum of a real transducer as well as our simulated spectrum is not a Gaussian function, going to zero at zero frequency. Hence, as the attenuation was increased and the scattered spectrum shifted to a lower frequency limit, the bandwidth of the Gaussian spectrum was also narrowed due to the attenuation

as the spectrum approached this lower limit. The algorithm did not include this possible change in the spectrum and thus failed.

One modification to the algorithm that was also considered to correct for its failure involved replacing the Gaussian spectrum approximation with a modified Rayleigh spectrum approximation that at least would go to zero at zero frequency (i.e., matching the theoretical analysis to the generated spectrum). The derivation leading to Eq. (4) would remain the same except for a multiplication of $|f|^4$ before the exponential. Then, the change in bandwidth would be found by fitting a modified Rayleigh distribution to the appropriate measured spectrum and solving for the scatterer size appropriately. Unfortunately, fitting Rayleigh functions to the measured spectrum was not a robust operation. Hence, changes in the attenuation still resulted in inappropriate changes in the bandwidth, and the algorithm still failed.

III. SPECTRAL FIT ALGORITHM

The goal of the SF algorithm was the same as that for the GT algorithm, that is, estimate the scatterer size and total attenuation from the *in vivo* backscattered power spectrum. Unlike the GT algorithm approach for which the *in vivo* backscattered power spectrum was assumed to be Gaussian distributed, there was no such assumption with the SF algorithm. Instead, a single minimization routine was used to fit a curve to the *in vivo* backscattered power spectrum, hence its name. The analysis is similar to the traditional method by Insana *et al.* (1990), who fitted the spectrum of the backscattered rf echoes from the region of interest (ROI) to an appropriate reference spectrum. And, unlike the approach by He and Greenleaf (1986), who used the entire backscattered rf echo where tissue heterogeneities along the propagation path would introduce errors, only the echoes from the ROI were needed to obtain the estimates of scatterer size and attenuation. Hence, tissue heterogeneity along the propagation path would not affect the estimates.

A. Overview of algorithm

The first step in the implementation of the SF algorithm is to estimate the theoretical value of $E[|V_{\text{refl}}|^2]$ from measured backscattererd rf echoes. In this work, $E[|V_{\text{refl}}|^2]$ was estimated by averaging the power spectra from 25 rf echoes in the log domain, that is

$$E[|V_{\text{refl}}(f)|^2] \approx P_{\text{scat}}(f) = \exp\left(\frac{1}{25} \sum_{j=1}^{25} \ln(|V_j|^2) \right). \quad (11)$$

The averaging removes the spectral fluctuation that results from the random scatterer spacing that masks the true value of $E[|V_{\text{refl}}|^2]$. The averaging was done in the log domain because it was assumed that the transmitted pulse was convolved with the random medium to generate the reflected spectrum. Hence, the spectral fluctuation from the random scatterer spacing should be included as a multiplicative random impulse train in the frequency domain [i.e., $|V_{\text{refl}}(f)|^2 = E[|V_{\text{refl}}|^2]|N_{\text{space}}(f)|^2$]. Multiplicative random variations can be removed by taking the log of the measured signals, so that the noise becomes additive, and then averaging.

In addition to estimating $E[|V_{\text{refl}}|^2]$, the SF algorithm requires a reference spectrum from a known reflector. In this work, the reference spectrum was obtained using the echo signal from a plane positioned at the focus. The echo from the plane was windowed by the same Hamming window used to window the simulated backscattered signal, and multiplied by k_o^4, yielding

$$P_{\text{ref}}(f) = k_o^4 |V_{\text{inc}}(\omega)|^2 |H(\omega)|^4 \propto k_o^4 |V_{\text{plane}}(\omega)|^2. \quad (12)$$

Once P_{scat} and P_{ref} had been determined, the scatterer size, a_{eff}, and total attenuation along the propagation path, α_o, were then found by estimating the values of a_{eff} and α_o that minimized the error given by

$$\text{ASD} = \underset{f}{\text{mean}}[(X(f, a_{\text{eff}}, \alpha_o) - \overline{X}(a_{\text{eff}}, \alpha_o))^2], \quad (13)$$

where

$$X(f, a_{\text{eff}}, \alpha_o) = \ln\left(\frac{P_{\text{scat}}(f)}{\max_f(P_{\text{scat}}(f))} \right) - \ln\left(\frac{P_{\text{ref}}(f) F_\gamma(f, a_{\text{eff}}) e^{-4\alpha_o f z_T}}{\max_f(P_{\text{ref}}(f) F_\gamma(f, a_{\text{eff}}) e^{-4\alpha_o f z_T})} \right),$$
$$\overline{X}(a_{\text{eff}}, \alpha_o) = \underset{f}{\text{mean}}[X(f, a_{\text{eff}}, \alpha_o)]. \quad (14)$$

Hence, the algorithm involved directly fitting a modified reference spectrum to the measured backscattered spectrum from the tissue region (i.e., spectral fitting). The fitting procedure is very similar to that described by Insana *et al.* (1990), when the attenuation is known. However, as implemented herein, two parameters are estimated instead of only a_{eff}. Fortunately, Eq. (13) has one minimum, as was confirmed by plotting the minimization surface for many different cases, so a simple minimization routine can be utilized.

B. Simulation results without electronic noise

The performance of the SF algorithm was also evaluated by simulations that were designed to test its performance as a function of attenuation. The same simulated scattered signals used to test the GT algorithm were used to test the SF algorithm. Hence, 40 independent estimates of scatterer size and attenuation were found per case for cases with homogeneous half-spaces with attenuation values between 0 and 1 dB/cm-MHz. When fitting the spectra [Eq. (13)], the SF algorithm used all spectral values greater than -30 dB relative to the value at the spectral peak. The choice of -30 dB for the limiting bandwidth is somewhat arbitrary; however, smaller bandwidths would reduce the amount of data available when performing the fit. The results for an attenuation of 0.3 dB/cm-MHz for the Hamming window lengths in the absence of electronic noise are shown in Fig. 2. The error bars are the same as those defined by Eq. (9) and Eq. (10). For the larger window lengths, the algorithm provided a reasonable estimate for scatterer size and total attenuation. However, as the window length was decreased, both the accuracy and precision degraded. The loss of accuracy was due to the convolution effects of the windowing function (Akita and Ueda, 1988). The loss of precision at smaller window

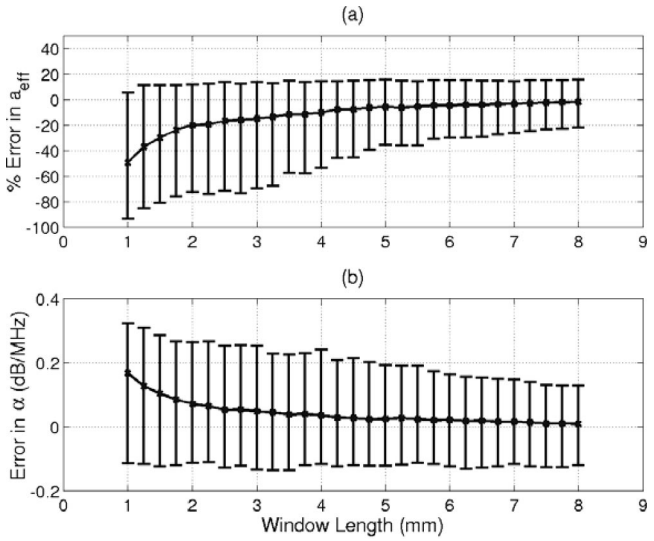

FIG. 2. Errors in estimates of (a) scatterer size and (b) total attenuation for different Hamming window lengths for an attenuation of 0.3 dB/cm-MHz in the absence of any electronic noise using the spectral fit algorithm.

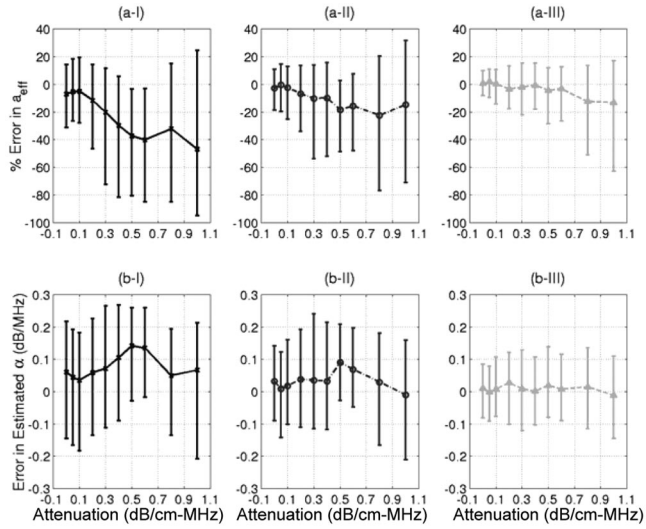

FIG. 3. Errors in estimates of (a) scatterer size and (b) total attenuation for different values of attenuation with Hamming window lengths of (I) 2 mm; (II) 4 mm; and (III) 8 mm in the absence of any electronic noise using the spectral fit algorithm.

lengths was probably due to a reduction in the number of independent samples in the least-squares fit [Eq. (13)] due to a loss in the frequency resolution of the spectrum (Wear 2001). The degradation with window length was also observed for other attenuation values (Fig. 3). The precision of the attenuation estimate, as well as the accuracy and precision of the scatterer size estimate, degraded with increasing attenuation. However, the average of all 40 estimates (i.e., accuracy) had errors smaller than 20% for the estimate of scatterer size and errors less than 0.2 dB/MHz for the attenuation estimate for all attenuation values and window lengths greater than 4 mm. An error of 0.2 dB/MHz translates to an error of about 20% when estimating the pressure amplitude at 8 MHz.

C. Electronic noise compensation

Although the accuracy results (Figs. 2 and 3) appear promising, the SF algorithm still needs to be evaluated in the presence of electronic system noise because real measurement systems will have noise. The effect of noise is twofold. First, the noise will reduce the usable bandwidth of the backscattered spectrum. The selection of the usable frequency range in the presence of noise for our work will be discussed in the next section. The second impact of electronic noise is a slight broadening of the backscattered spectrum. This broadening must be compensated before accurate estimates can be obtained from the noisy waveform.

In order to understand the broadening, assume that the electronic noise is additive, white, and with zero mean. Then, the expected spectrum over the set of possible additive noise for a given scatterer distribution is given by

$$E_N[|V_{\text{refl}}(f)+N(f)|^2]=|V_{\text{refl}}(f)|^2E_N\left[\left|1+\frac{N(f)}{V_{\text{refl}}(f)}\right|^2\right]$$
$$=|V_{\text{refl}}(f)|^2\left(1+\frac{E_N[|N(f)|^2]}{|V_{\text{refl}}(f)|^2}\right). \tag{15}$$

The values near the peak of $|V_{\text{refl}}|^2$ are not affected by the noise while the $|V_{\text{refl}}|^2$ values near the edge of the usable spectrum are increased resulting in a broadening of the spectrum.

In order to compensate for the spectral broadening from the noise, consider $P_{\text{scat}}(f)$ obtained from averaging the spectra in the log domain in the presence of noise given by

$$P_{\text{scat}}(f)=\exp\left(\frac{1}{25}\sum_{i=1}^{25}\ln\left(|V_i(f)|^2\left(1+\frac{E_N[|N(f)|^2]}{|V_i(f)|^2}\right)\right)\right)=P_{\text{scat}}(f)|_{\text{ideal}}\exp\left(\frac{1}{25}\sum_{i=1}^{25}\ln\left(1+\frac{E_N[|N(f)|^2]}{|V_i(f)|^2}\right)\right)$$
$$\cong P_{\text{scat}}(f)|_{\text{ideal}}\exp\left(\ln\left(1+\frac{1}{25}\sum_{i=1}^{25}\frac{E_N[|N(f)|^2]}{|V_i(f)|^2}\right)\right)\cong P_{\text{scat}}(f)|_{\text{ideal}}\exp\left(\ln\left(1+\frac{E_N[|N(f)|^2]}{\frac{1}{25}\sum_{i=1}^{25}|V_i(f)|^2}\right)\right)$$
$$=P_{\text{scat}}(f)|_{\text{ideal}}\left(1+\frac{E_N[|N(f)|^2]}{\frac{1}{25}\sum_{i=1}^{25}|V_i(f)|^2}\right)\cong P_{\text{scat}}(f)|_{\text{ideal}}\left(1+\frac{E_N[|N(f)|^2]}{P_{\text{scat}}(f)|_{\text{ideal}}}\right), \tag{16}$$

where $P_{\text{scat}}(f)|_{\text{ideal}}$ equals $P_{\text{scat}}(f)$ in the absence of noise. $E_N[|N(f)|^2]$ can be determined for the experimental system by recording the noise in the absence of a transmitted signal and then taking the mean value of $|N(f)|^2$. The effect of electronic noise can then be reduced by dividing $P_{\text{scat}}(f)$ by $(1+E_N[|N(f)|^2]/P_{\text{scat}}(f))$ before solving for the scatterer size and attenuation assuming that $P_{\text{scat}}(f)|_{\text{ideal}} \cong P_{\text{scat}}(f)$. Compensating for the electronic noise using this term is similar to the SNR weighting described previously by Oelze and O'Brien (2002b) only without their accompanying loss of bandwidth. Comparisons of the accuracy of the estimates (i.e., average of all 40 estimates) both with and without the electronic noise compensation are provided in Fig. 4 for three SNR values (9, 23, and 36 dB) calculated from

$$\text{SNR} = \frac{1}{25}\sum_{j=1}^{25}\left(10\cdot\log\left(\frac{\int(g_{\text{win}}(t)v_{\text{refl}_j}(t))^2dt}{\int(g_{\text{win}}(t)v_{\text{noise}}(t))^2dt}\right)\right), \quad (17)$$

where v_{refl_j} are from each group of 25 rf echoes used in the estimate before the noise was added, and v_{noise} is the noise signal used to obtain the estimate for $E_N[|N(f)|^2]$. The SNR values in the legend are the average values from all 40 data sets [Eq. (17)]. Accurate estimates of both scatterer size (~10%) and attenuation (~0.15 dB/MHz) were obtained using the noise compensation for all three levels of electronic noise, while the estimates without the noise compensation quickly degraded with increasing noise. Even SNRs as high as 23 dB had errors of 20% in the scatterer size estimate in the absence of noise compensation.

D. Simulation results with electronic noise

The effect of electronic noise on the SF algorithm was evaluated by adding white Gaussian noise of varying levels to the simulated rf echoes in the time domain. The power of the random noise signal was set relative to the reference signal from the rigid plane placed at the focal plane. Also, one of the randomly generated noise signals in the time domain for each noise level was used to calculate $E_N[|N(f)|^2]$ for the noise compensation. In order to not bias the estimates by using frequencies dominated by noise, the fit used all frequencies corresponding to signal values satisfying

$$\left\{10\log\left(\frac{P_{\text{scat}}(f)}{\max_{\forall f}(P_{\text{scat}}(f))}\right)\right\}_{\substack{\text{polynomial}\\ \text{fit}}} > \max\left(\left[-30\ \ \text{mean}\left(\left\{10\log\left(\frac{P_{\text{scat}}(f)}{\max_{\forall f}(P_{\text{scat}}(f))}\right)\right\}_{\substack{\text{polynomial}\\ \text{fit}}}\right)\right]\right), \quad (18)$$

where the spectra were fit by a polynomial of large degree to reduce the impact of spectral variations on the selected frequency range. The backscattered signal was significantly oversampled (i.e., sampling frequency of 53 MHz was ~4 times the Nyquist frequency), so that the mean of the spectrum would yield a value slightly larger than the level of the white zero-mean random noise. Therefore, Eq. (18) only selected signal values greater than the noise floor of the system. Although the degree of the polynomial is arbitrary, a value of 50 was used. Other values considered did not have a significant impact on the final results.

For each noise level and for half-space attenuation values between 0.05 and 1 dB/cm-MHz, the scatterer size and total attenuation were estimated for Hamming window lengths from 1 to 8 mm. The simulation results with half-space attenuation values of 0.3, 0.6, and 1 dB/cm-MHz are shown in Figs. 5, 6, and 7, respectively. The vertical error

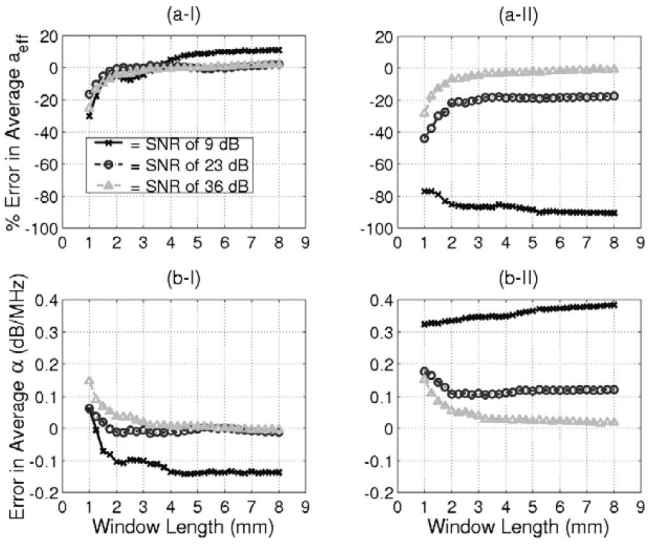

FIG. 4. Errors in estimates of (a) scatterer size and (b) total attenuation both (I) with and (II) without noise compensation for a half-space with an attenuation of 0.05 dB/cm-MHz using the spectral fit algorithm.

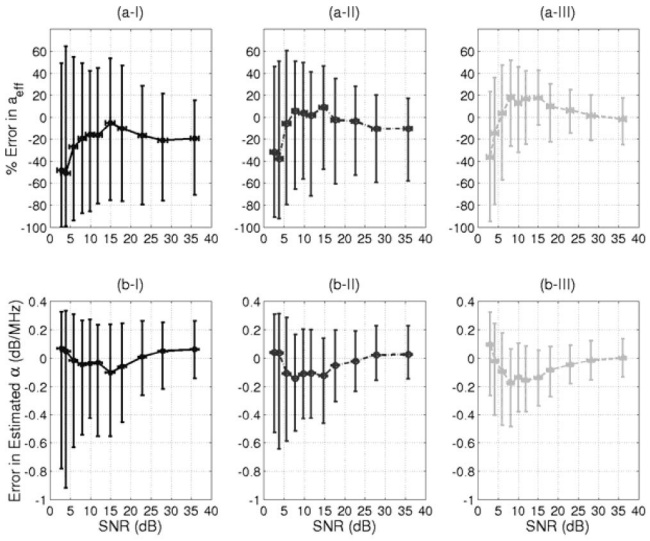

FIG. 5. Errors in estimates of (a) scatterer size and (b) total attenuation for different levels of electronic noise for a half-space attenuation of 0.3 dB/cm-MHz and Hamming window lengths of (I) 2 mm; (II) 4 mm; and (III) 8 mm using the spectral fit algorithm.

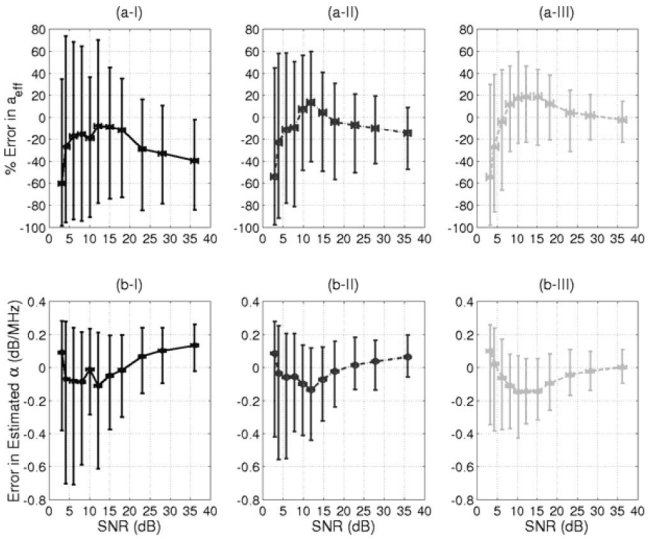

FIG. 6. Errors in estimates of (a) scatterer size and (b) total attenuation for different levels of electronic noise for a half-space attenuation of 0.6 dB/cm-MHz and Hamming window lengths of (I) 2 mm; (II) 4 mm; and (III) 8 mm using the spectral fit algorithm.

bars are the same as those given in Eq. (9) and Eq. (10), and the horizontal error bars correspond to plus and minus 1 standard deviation of the calculated SNR values from Eq. (17) from each of the 40 estimates.

The SF algorithm gives reasonably accurate average estimates of the scatterer size with errors less than 20% for SNRs between 6 and 36 dB for half-space attenuation values between 0.05 and 1 dB/cm-MHz and window lengths greater than 4 mm. Likewise, the average estimate for the total attenuation had errors less than 0.2 dB/MHz for SNRs between 3 and 36 dB. Unfortunately, the algorithm is not very precise as can be seen from the large error bars about the average estimates. As a result, consistently precise estimates (i.e., error bars $<$20% for size estimates and $<$0.2 dB/MHz for attenuation estimates) can only be obtained for SNRs better than 23 dB for half-space attenuation values between 0.05 and 0.3 dB/cm-MHz and better than 28 dB for half-space attenuation values between 0.4 and 0.6 dB/cm-MHz for the window length of 8 mm. The higher values of half-space attenuation never meet this precision limit. Furthermore, the precision of the smaller window lengths is worse.

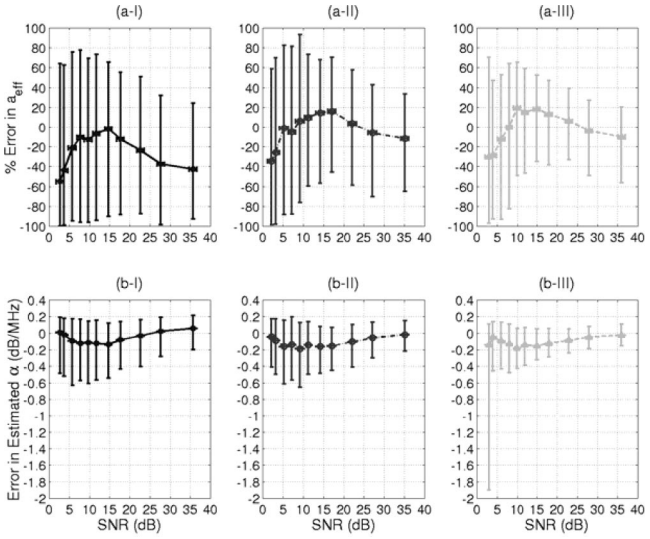

FIG. 7. Errors in estimates of (a) scatterer size and (b) total attenuation for different levels of electronic noise for a half-space attenuation of 1 dB/cm-MHz and Hamming window lengths of (I) 2 mm; (II) 4 mm; and (III) 8 mm using the spectral fit algorithm.

IV. DISCUSSION

The performance of two algorithms for estimating the scatterer size and total attenuation simultaneously from the same set of backscattered waveforms has been assessed. The first was the Gaussian transformation algorithm, which treated the scatterer size and attenuation as two different Gaussian transformations operating on the Gaussian-distributed backscattered spectrum. Although the algorithm's performance was reasonable for very small attenuation values, the accuracy of the scatterer size estimate quickly degraded with increasing attenuation. The failure was a result of the algorithm assuming that the bandwidth of the spectrum was only affected by the scatterer size, an approximation that would be true for a purely Gaussian spectrum. However, the spectrum of a real transducer is also narrowed due to the attenuation as the spectrum is shifted towards zero frequency. It is thus concluded that it is unlikely that any algorithm that makes approximations regarding the shape of the spectra will yield accurate results when estimating both the scatterer size and total attenuation from the *in vivo* backscattered power spectrum, even though the approximations are valid in other applications (Wear, 2002). Algorithms that make an assumption about the shape of the spectrum restrict its applicability by limiting any type of spectral coding that may be added to improve noise performance. Hence, the other algorithm considered did not make any assumption about the spectrum.

The second algorithm investigated was the spectral fit algorithm. Although the accuracy of the algorithm (i.e., average value of estimates) was reasonable for SNRs between 6 and 36 dB and half-space attenuation values between 0.05 and 1 dB/cm-MHz for Hamming window lengths greater than 4 mm, the precision was only reasonable for SNRs between 23 and 36 dB for half-space attenuation values of 0.05 and 0.3 dB/cm-MHz and SNRs between 28 and 36 dB for half-space attenuation values from 0.4–0.6 dB/cm-MHz at window lengths of 8 mm. The precision degraded with increasing noise, decreasing window length, and increasing attenuation. Although the SF algorithm is very similar to the established method for determining just the scatterer size when the attenuation is known (Insana *et al.*, 1990), the accuracy and precision of the estimates have been degraded by the need to estimate two parameters instead of just one.

Even though the SF algorithm is not as precise as the traditional method where the attenuation is known, the amount of data (i.e., window length and number of rf echoes) needed to obtain reasonable estimates can be compared to the amount of data typically used to obtain estimates of the scatterer size and attenuation independently. The window length typically used when estimating scatterer size in this frequency range has varied from 2.5 to 16 mm (Oelze *et al.*, 2002), while Insana *et al.* (1995) obtained consistent results using a window length of 7.9 mm. Hence, using a window

length of 4 to 8 mm is reasonable over this frequency range. Similarly, a typical number of rf echoes used in the estimate has been 14 (Insana *et al.*, 1995) and 20 (Oelze *et al.*, 2002), on the same order as the 25 echoes used herein. When estimating the attenuation independently, the concept of window length does not apply because typically a very short window is used throughout the ROI (Baldeweck *et al.*, 1994). However, the number of rf echoes required to obtain precise attenuation estimates can still be compared. In the past, 256 echoes have been used when estimating attenuation (Baldeweck *et al.*, 1994; D'Astous and Foster, 1986), considerably more than the 25 echoes used for each estimate herein. The precision of the SF algorithm would be improved if 256 echoes were used per estimate instead of the 25. We decided to only use 25 echoes so that the results would be more comparable to what is currently done in QUS imaging.

Although the precision of the SF algorithm still has challenges, the robustness of the average estimates (i.e., accuracy) allows for improved quantification of the tissue properties. Consider the estimate of scatterer size for a tumor. Typically, estimates are obtained throughout the tumor and then averaged together in order to obtain a final size estimate for classifying the tumor (Oelze *et al.*, 2004). Hence, if the tumor was large enough to allow for many different estimates to be obtained from the SF algorithm and averaged, the final estimate would be very close to the true characteristic size for the tumor and would not be affected by any intervening tissue layers.

The situation is similar when quantifying acoustic radiation force impulse imaging (Nightingale *et al.*, 2000) or patient-specific dosimetry (Siddiqi *et al.*, 1992). In both applications, the intensity of the ultrasound, obtainable from the total attenuation, is the only quantity that cannot be estimated using established methods. However, the total attenuation at a particular tissue depth will not normally change drastically for neighboring tissue regions. Therefore, estimates from the SF algorithm could be averaged from neighboring tissue regions to obtain a more accurate estimate of the total attenuation. The size of the region over which the total attenuation estimates could be averaged without biasing the results is a subject of further study beyond the scope of this paper. As an added benefit, it may be possible to combine the scatterer size estimate also obtained from the SF algorithm with acoustic radiation force impulse imaging to develop a multiparameter, noninvasive diagnostic tool.

ACKNOWLEDGMENTS

This work was supported by the University of Illinois Research Board, by a NDSEG Fellowship awarded to T. A. Bigelow, and by a Beckman Institute Graduate Fellowship awarded to T. A. Bigelow.

Akita, M., and Ueda, M. (**1988**). "The effects of windowing on spectral estimation of echoes scattered by a random medium," J. Acoust. Soc. Am. **107**, 1243–1248.

Baldeweck, T., Herment, A., Laugier, P., and Berger, G. (**1994**). "Attenuation estimation in highly attenuating media using high frequencies: A comparison study between different meant frequency estimators," IEEE Ultrason. Symp., 1783–1786.

Bigelow, T. A., and O'Brien, Jr., W. D. (**2004**). "Scatterer size estimation in pulse–echo ultrasound using focused sources: Theoretical approximations and simulation analysis," J. Acoust. Soc. Am. **116**, 578–593.

Chaturvedi, P., and Insana, M. F. (**1996**). "Error bounds on ultrasonic scatterer size estimates," J. Acoust. Soc. Am. **100**, 392–399.

D'Astous, F. T., and Foster, F. S. (**1986**). "Frequency dependence of ultrasound attenuation and backscatter in breast tissue," Ultrasound Med. Biol. **12**, 795–808.

Dussik, K. T., and Fritch, D. J. (**1956**). "Determination of sound attenuation and sound velocity in the structures constituting the joints, and of the ultrasonic field distribution within the joints on living tissues and anatomical preparations, both in normal and pathological conditions," Public Health Service, Nat. Inst. Health Project A454, Progr. Report.

Goss, S. A., Johnston, R. L., and Dunn, F. (**1978**). "Compilation of empirical ultrasonic properties of mammalian tissues," J. Acoust. Soc. Am. **64**, 423–457.

Goss, S. A., Johnston, R. L., and Dunn, F. (**1980**). "Compilation of empirical ultrasonic properties of mammalian tissues. II," J. Acoust. Soc. Am. **68**, 93–108.

Hall, T. J., Insana, M. F., Harrison, L. A., and Cox, G. G. (**1996**). "Ultrasonic measurement of glomerular diameters in normal adult humans," Ultrasound Med. Biol. **22**, 987–997.

He, P., and Greenleaf, J. F. (**1986**). "Application of stochastic analysis to ultrasonic echoes—estimation of attenuation and tissue heterogeneity from peaks of echo envelope," J. Acoust. Soc. Am. **79**, 526–534.

Insana, M. F., Wagner, R. F., Brown, D. G., and Hall, T. J. (**1990**). "Describing small-scale structure in random media using pulse–echo ultrasound," J. Acoust. Soc. Am. **87**, 179–192.

Insana, M. F., Wood, J. G., Hall, T. J., Cox, G. G., and Harrison, L. A. (**1995**). "Effects of endothelin-1 on renal microvasculature measured using quantitative ultrasound," Ultrasound Med. Biol. **21**, 1143–1151.

Jongen, H. A. H., Thijssen, J. M., Aarssen, M., and Verhoef, W. A. (**1986**). "A general model for the absorption of ultrasound by biological tissues and experimental verification," J. Acoust. Soc. Am. **79**, 535–540.

Lizzi, F. L., Greenebaum, M., Feleppa, E. J., and Elbaum, M. (**1983**). "Theoretical framework for spectrum analysis in ultrasonic tissue characterization," J. Acoust. Soc. Am. **73**, 1366–1373.

Lizzi, F. L., Astor, M., Liu, T., Deng, C., Coleman, D. J., and Silverman, R. H. (**1997**). "Ultrasonic spectrum analysis for tissue assays and therapy evaluation," Int. J. Imaging Syst. Technol. **8**, 3–10.

Lu, Z. F., Zagzebski, J. A., and Lee, F. T. (**1999**). "Ultrasound backscatter and attenuation in human liver with diffuse disease," Ultrasound Med. Biol. **25**, 1047–1054.

Nassiri, D. K., and Hill, C. R. (**1986**). "The use of angular acoustic scattering measurements to estimate structural parameters of human and animal tissues," J. Acoust. Soc. Am. **79**, 2048–2054.

Nightingale, K. L., Nightingale, R. W., Palmer, M. L., and Trahey, G. E. (**2000**). "A finite element model of remote palpation of breast lesions using radiation force: Factors affecting tissue displacement," Ultrason. Imaging **22**, 35–54.

Oelze, M. L., and O'Brien, Jr., W. D. (**2002a**). "Frequency-dependent attenuation-compensation functions for ultrasonic signals backscattered from random media," J. Acoust. Soc. Am. **111**, 2308–2319.

Oelze, M. L., and O'Brien, Jr., W. D. (**2002b**). "Method of improved scatterer size estimation and application to parametric imaging using ultrasound," J. Acoust. Soc. Am. **112**, 3053–3063.

Oelze, M. L., Zachary, J. F., and O'Brien, Jr., W. D. (**2002**). "Characterization of tissue microstructure using ultrasonic backscatter: Theory and technique for optimization using a Gaussian form factor," J. Acoust. Soc. Am. **112**, 1202–1211.

Oelze, M. L., O'Brien, Jr., W. D., Blue, J. P., and Zachary, J. F. (**2004**). "Differentiation and characterization of rat mammary fibroadenomas and 4T1 mouse carcinomas using quatitative ultrasound imaging," IEEE Trans. Med. Imaging **23**, 764–771.

Siddiqi, T. A., O'Brien, Jr., W. D., Meyer, R. A., Sullivan, J. M., and Miodovnik, M. (**1992**). "Human *in situ* dosimetry: Differential insertion loss during passage through abdominal wall and myometrium," Ultrasound Med. Biol. **18**, 681–689.

Wear, K. A. (**2001**). "Fundamental precision limitations for measurements of frequency dependence of backscatter: Applications in tissue mimicking phantoms and trabecular bone," J. Acoust. Soc. Am. **110**, 3275–3282.

Wear, K. A. (**2002**). "A Gaussian framework for modeling effects of frequency-dependent attenuation, frequency-dependent scattering, and gating," IEEE Trans. Ultrason. Ferroelectr. Freq. Control **49**, 1572–1582.